

# Co-modified MCM-41 as an effective adsorbent for levofloxacin removal from aqueous solution: *optimization of process parameters, isotherm, and thermodynamic studies*

Ting Jin<sup>1</sup> · Wenhua Yuan<sup>1</sup> · Yujie Xue<sup>1</sup> · Hong Wei<sup>2</sup> · Chaoying Zhang<sup>1</sup> · Kebin Li<sup>1</sup>

Received: 20 October 2016 / Accepted: 13 December 2016 / Published online: 21 December 2016  
© Springer-Verlag Berlin Heidelberg 2016

**Abstract** Antibiotics are emerging contaminants due to their potential risks to human health and ecosystems. Poor biodegradability makes it necessary to develop effective physical-chemical methods to eliminate these contaminants from water. The cobalt-modified MCM-41 was prepared by a one-pot hydrothermal method and characterized by SAXRD, N<sub>2</sub> adsorption-desorption, SEM, UV–Vis DR, and FTIR spectroscopy. The results revealed that the prepared 3% Co-MCM-41 possessed mesoporous structure with BET surface areas at around 898.5 m<sup>2</sup>g<sup>-1</sup>. The adsorption performance of 3% Co-MCM-41 toward levofloxacin (LVF) was investigated by batch experiments. The adsorption of LVF on 3% Co-MCM-41 was very fast and reached equilibrium within 2 h. The adsorption kinetics followed the pseudo-second-order kinetic model with the second-order rate constants in the range of 0.00198–0.00391 g mg<sup>-1</sup> min<sup>-1</sup>. The adsorption isotherms could be well represented by the Langmuir, Freundlich, and Dubinin-Radushkevich (D-R) isotherm equations. Nevertheless, D-R isotherm provided the best fit based on the coefficient of determination and average relative error values. The mean free energy of adsorption (*E*) calculated from D-R model was

about 11 kJ mol<sup>-1</sup>, indicating that the adsorption was mainly governed by a chemisorption process. Moreover, the adsorption capacity was investigated as a function of pH, adsorbent dosage, LVF concentration, and temperature with help of respond surface methodology (RSM). A quadratic model was established, and an optimal condition was obtained as follows: pH 8.5, adsorbent dosage of 1 g L<sup>-1</sup>, initial LVF concentration of 119.8 mg L<sup>-1</sup>, and temperature of 31.6 °C. Under the optimal condition, the adsorption capacity of 3% Co-MCM-41 to LVF could reach about 108.1 mg g<sup>-1</sup>. The solution pH, adsorbent dosage, LVF concentration, and a combination of adsorbent dose and LVF concentration were significant factors affecting the adsorption process. The adsorption thermodynamic functions were also determined. The negative  $\Delta H^0$  (–33.50 kJ mol<sup>-1</sup>) and  $\Delta S^0$  (–43.57 J mol<sup>-1</sup> K<sup>-1</sup>) suggested that the adsorption was an exothermic process accompanied by decreasing disorder. This study may indicate that 3% Co-MCM-41 is a promising adsorbent for removing emerging pollutants of LVF from water.

**Keywords** Adsorption · Cobalt-modified MCM-41 · Levofloxacin · Response surface methodology

Responsible editor: Guilherme L. Dotto

**Electronic supplementary material** The online version of this article (doi:10.1007/s11356-016-8262-0) contains supplementary material, which is available to authorized users.

✉ Kebin Li  
kebin68li@163.com

<sup>1</sup> Key Laboratory of the Ministry of Education for Synthetic and Natural Functional Molecule Chemistry, College of Chemistry and Material Science, Northwest University, Xi'an 710069, China

<sup>2</sup> State Key Laboratory Base of Eco-Hydraulic Engineering in Arid Areas, Xi'an University of Technology, Xi'an 710048, China

## Introduction

Fluoroquinolones (FQs) are a class of broad-spectrum antibacterial medicines, which are widely used in the treatment of both human and animal diseases. Based on annual global sales and therapeutic versatility, FQs represent one of the most important classes of antibacterial agents worldwide (Dodd et al. 2005). Levofloxacin (an active optical isomer of ofloxacin) is a more recently developed antibiotic, belonging to the third generation quinolones. The widespread use and the lack of treatment processes targeting these compounds are

resulting in their ubiquity in surface waters (Paul et al. 2007; Perini et al. 2016). Levofloxacin (LVF) has been detected in several surface waters at concentration levels up to  $87.4 \text{ ng L}^{-1}$  (Kim et al. 2009). The presence of antibiotics in the environment may alter microbial ecology, provokes the development of and spread of antibiotic-resistance, and even gives rise to unexpected effects on human health through food chain (Halling-Sorensen et al. 1998; Ali and Aboul-Enein 2004; Van Doorslaer et al. 2014; Serna-Galvis et al. 2016). Moreover, FQs have been confirmed to be toxic to plants and aquatic organism (Brain et al. 2004; Robinson et al. 2005) and to have the significant genotoxicity (Hartmann et al. 1998). It is thus of great importance to develop efficient and cost-effective treatment technologies for removal of such compounds from aquatic environments.

So far, several approaches such as photolysis (Paul et al. 2010), photocatalytic decomposition (Paul et al. 2010), adsorption (Ali 2010; Shi et al. 2013; Ali 2014; Jung et al. 2015; Masson et al. 2016), sonolysis (Wei et al. 2015), chlorination (Sharma 2008), ozonation (Witte et al. 2009), photo-Fenton degradation (Perini et al. 2016), and anodic Fenton treatment (Xiao et al. 2010) have been adopted to treat the antibiotic contaminated water. Among them, adsorption has proven to be an effective and promising process to remove micropollutants from aqueous solutions in view of its inexpensive nature and ease of operation (Zhang et al. 2010; Ali 2012; Ali et al. 2012; Shi et al. 2013; Masson et al. 2016).

However, up to now, only a few studies have been conducted to investigate adsorption of LVF or ofloxacin from aqueous solutions. Nowara et al. (1997) reported the adsorption of several FQs, including LVF to soil, soil clay fractions, and soil minerals. We studied the adsorption of LVF on Fe-pillared montmorillonite (Liu et al. 2015). Moreover, Djurdjevic et al. (2001) investigated the adsorption of ofloxacin by  $\text{Al}_2\text{O}_3$  solids. Goyne et al. (2005) examined ofloxacin adsorption to nonporous and mesoporous  $\text{Al}_2\text{O}_3$  and  $\text{SiO}_2$  mineral sorbents. Lately, Masson et al. (2016) reported the adsorption of ofloxacin and other organic pollutants using microporous-activated carbon fabric. In contrast, reports on adsorption of relatively older FQs such as ciprofloxacin and norfloxacin are abundant. Natural minerals (Li et al. 2011; Wu et al. 2010), metal oxide (Gu and Karthikeyan 2005), coal fly ash (Zhang et al. 2010), functionalized hexagonal mesoporous silicate (Punyapalakul and Sitthisorn 2010), activated carbon (Carabineiro et al. 2011), carbon nanotubes (Peng et al. 2012), magnetic mesoporous carbon nanocomposite (Shi et al. 2013), etc. have been used as potential adsorbents to explore ciprofloxacin adsorption. From these studies, one can see that surface area, texture, and composition are important factors affecting the adsorption performance of adsorbent to FQs.

MCM-41 is a member of the mesoporous molecular sieve M41S family. Because of a hexagonally arranged uniform pore structure, large specific surface area, and high thermal stability, MCM-41 is a very promising candidate of catalyst, catalyst

support, or adsorbents (Dimos et al. 2009; Chatterjee et al. 2014; Martins et al. 2016; Xu et al. 2016). MCM-41 and functionalized MCM-41 have been extensively used for adsorptive removal heavy metal ions and organic dyes (Ho et al. 2003; Benhamou et al. 2009; Dimos et al. 2009). However, the removal of emerging organic contaminants such as pharmaceutical antibiotics on mesoporous silica molecular sieves and related materials was seldom reported (Chen et al. 2015). Goyne et al. (2005) found that relative to the nonporous solid, the presence of intraparticle porosity resulted in a statistically significant sorption enhancement of silica to ofloxacin. In addition, it is well-known that quinolone antibiotics can form complexes with divalent cations. Inspired by these results, we expect that the incorporation of metal ions, such as cobalt ions, into MCM-41 will modify its adsorptive properties by improving its affinity to FQs.

Accordingly, cobalt-modified MCM-41 (Co-MCM-41) was synthesized by a solvothermal method, and the feasibility of adsorptive removal of LVF from aqueous solution by Co-MCM-41 was evaluated. The effects of the operational variables (pH, LVF concentration, temperature and adsorbent dose) and their interactions on the adsorption process were investigated by means of Box–Behnken design (BBD) under response surface methodology (RSM). The isotherms and thermodynamics were determined. Additionally, the prepared Co-MCM-41 was characterized by XRD,  $\text{N}_2$  adsorption/desorption, Fourier transform-infrared spectroscopy (FT-IT), diffuse reflectance UV–Vis spectroscopy, and scanning electron microscopy (SEM).

## Experimental

### Chemicals

Tetraethylorthosilicate (TEOS, 98% GC) and cetyltrimethyl ammonium bromide (CTAB, >99%) were purchased from Aldrich Chemical Inc. LVF (>99%,  $\text{C}_{18}\text{H}_{20}\text{FN}_3\text{O}_4$ ,  $361.368 \text{ g mol}^{-1}$ ) was obtained from Xinchang Pharmaceutical Factory (Zhejiang, China). All other reagents such as sodium hydroxide (NaOH) and cobalt nitrate ( $\text{Co}(\text{NO}_3)_2 \cdot 6\text{H}_2\text{O}$ ) were of analytical grade and obtained from Sinopharm Chemical Reagent Co. Ltd., China. Deionized water generated by a Millipore Mill-Q system was used throughout the study.

### Preparation of MCM-41 and Co-modified MCM-41 materials

The mesoporous silica MCM-41 was synthesized by hydrothermal method (Dimos et al. 2009). A typical synthesis procedure was as follows: 2.2 g of CTAB was dissolved in 52 g of deionized water as structure directing agent. Then, 10 mL of TEOS was added as the silica source under vigorous stirring. After a few minutes, 20 mL of ammonia solution (25 wt%)

was added into by dropwise. At this time, the solution became milky. After the white turbid suspension was further stirred at a certain speed for 2 h, the resulting suspensions were transferred into a stainless steel autoclave and hydrothermalized at 100 °C for 12 h. Subsequently, the solid product was recovered by filtration, washed two times with deionized water and ethanol, and dried at room temperature. The dry material was further calcined by heating to 550 °C for 5 h to remove the template (CTAB).

For cobalt-modified MCM-41 (Co-MCM-41) synthesis, the same procedure was used except that a certain amount of cobalt nitrate was added before introducing silica source. The molar ratios of TEOS/CTAB/Co/ammonia/H<sub>2</sub>O were (1-*x*):0.11:0.22:*x*:100 (*x* = 0.01, 0.02, and 0.03, respectively). According to these ratios, different reactants were added in the reaction solutions. The obtained products were denoted as *x*% Co-MCM-41, where *x* stands for the nominal atomic percentage ratio of Co to Si in synthesis solutions.

### Adsorption experiments

The adsorption experiments were performed in a batch mode. A typical experimental procedure was as follows: a certain amount of adsorbents was weighed into 100-mL stopper conical flask. Then, 50 mL of LVF solution with a known concentration and initial pH value was taken in. After being sealed, the flask was put into a thermostatic shaker and shaken at 150 rpm. At the predetermined time, the flask was withdrawn and the adsorbent was separated. The residual concentration of LVF in the supernatant was determined using a UV-visible spectrophotometer. If necessary, the pH of solution was adjusted by 1 mol L<sup>-1</sup> NaOH or HNO<sub>3</sub> solutions.

For kinetic experiments, a series of 50 mL of LVF solutions with a known concentration (80, 100, or 120 mg L<sup>-1</sup>) was contacted with 0.025 g of the sorbent at 25 °C. At the present time, the residual concentration of LVF in the solution was determined. In the case of adsorption isotherm determination, 50-mL LVF solutions with different initial concentrations (20–120 mg L<sup>-1</sup>) were agitated with 0.025 g of sorbent at a given temperature for 5 h to establish equilibrium. To examine the effects of process variables, such as adsorption dose (*m*), LVF concentration (*C*), temperature (*T*), and initial pH of solution on LVF adsorption, RSM was employed. The experimental conditions followed the designed values (see Table 1).

In most cases, each experiment was performed at least in duplicate under identical conditions and the average values were presented. The relative errors of the data were about 3.5%. The blank experiment (without adsorbent) indicated that adsorption of the bottle wall and losses during sample

treatment were negligible. Therefore, the amount of adsorbed LVF (*q*, mg g<sup>-1</sup>) was calculated from the difference in concentration between the initial and after adsorption by Eq. (1):

$$q = \frac{(C_0 - C_t)V}{m} \quad (1)$$

where *C*<sub>0</sub> and *C*<sub>*t*</sub> (mg L<sup>-1</sup>) are the concentration of LVF initially and a certain time (min), respectively. *V* is the volume of solution (L), and *m* is the mass of adsorbent (g).

### Experimental design

RSM is a combination of mathematical and statistical technique that is extensively used in process optimizing and modeling. In addition, it is also capable of revealing the relative significance and their interaction of several affecting factors (Roosta et al. 2015; Azzaz et al. 2016). Therefore, a three-level four-factorial Box–Behnken design under RSM was applied to investigate the effects of adsorption dose (*m*), LVF concentration (*C*), temperature (*T*), and pH on LVF adsorption. The range and levels in the experiments were decided on basis of our preliminary single factor experiments. Three levels were chosen for each variable. A complete experimental design matrix along with the coded values of variables and their real values is presented in Table 1. The statistical software of Design-Expert (Trail version 8, State-Ease, Inc., MN, and USA) was used for designing and analyzing the experimental data.

### Physical and chemical analyses

X-ray powder diffraction (XRD) analysis was carried on a D8 Advance X-ray diffractometer (Bruker, Germany) with Cu Kα radiation source ( $\lambda = 1.5418 \text{ \AA}$ ) scanning from  $2\theta = 1^\circ$  to  $9^\circ$ . N<sub>2</sub> adsorption/desorption isotherms were measured at 77.4 K using Micromeritic TriStar II 3020 analyzer. Prior to measurement, samples were degassed at 200 °C for 5 h. The pore size distribution was calculated from the adsorption branch of the isotherm using the Barrett–Joyner–Helenda (BJH) method. Fourier transformed infrared (FT-TIR) spectra were recorded on a Bruker TENSIR27 FT-IR spectrometer. The samples were dispersed in KBr pellet. Ultraviolet-visible (UV–Vis) diffuse reflectance spectroscopy (DRS) was carried out on a Shimadzu UV2550 spectrometer using BaSO<sub>4</sub> as the reference and converted to absorption spectra according to the Kubelka–Munk method. SEM analysis was performed on a SU-8010 field emission SEM microscope (Hitachi, Japan).

The concentration of LVF was measured by a UV–Vis spectrophotometer (Shimadzu UV2550). The spectrum of LVF solution varies with pH but is fairly constant below and above 5.6. Thereby, two sets of calibration curves were

**Table 1** Box–Behnken design matrix along with observed response for LVF removal

Run	Coded				Real				Adsorption capacity (mg g <sup>-1</sup> )
	pH, $x_1$	Dosage (g/50 mL), $x_2$	Temp. (°C), $x_3$	LVF conc. (mg L <sup>-1</sup> ), $x_4$	pH	Dosage (g/50 mL), $m$	Temp. (°C), $T$	LVF conc. (mg L <sup>-1</sup> ), $C$	
1	0	-1	0	1	7.0	0.05	50.0	100.0	86.2
2	0	0	0	0	7.0	0.07	35.0	100.0	64.9
3	0	0	0	0	7.0	0.07	35.0	100.0	65.4
4	0	-1	-1	0	7.0	0.05	35.0	80.0	71.2
5	0	1	-1	0	7.0	0.09	35.0	80.0	41.8
6	0	1	0	1	7.0	0.09	50.0	100.0	51.8
7	1	1	0	0	9.0	0.09	35.0	100.0	52.6
8	0	0	-1	1	7.0	0.07	50.0	80.0	52.2
9	0	0	0	0	7.0	0.07	35.0	100.0	66.8
10	1	-1	0	0	9.0	0.05	35.0	100.0	90.5
11	-1	0	-1	0	5.0	0.07	35.0	80.0	49.3
12	0	0	1	1	7.0	0.07	50.0	120.0	77.6
13	-1	0	0	-1	5.0	0.07	20.0	100.0	55.9
14	-1	0	0	1	5.0	0.07	50.0	100.0	48.0
15	0	1	1	0	7.0	0.09	35.0	120.0	62.5
16	0	0	1	-1	7.0	0.07	20.0	120.0	78.5
17	1	0	0	1	9.0	0.07	50.0	100.0	63.5
18	1	0	1	0	9.0	0.07	35.0	120.0	81.3
19	-1	1	0	0	5.0	0.09	35.0	100.0	50.5
20	0	1	0	-1	7.0	0.09	20.0	100.0	51.8
21	0	0	-1	-1	7.0	0.07	20.0	80.0	53.2
22	-1	-1	0	0	5.0	0.05	35.0	100.0	83.4
23	0	0	0	0	7.0	0.07	35.0	100.0	65.3
24	1	0	0	-1	9.0	0.07	20.0	100.0	66.4
25	0	-1	0	-1	7.0	0.05	20.0	100.0	90.1
26	0	0	0	0	7.0	0.07	35.0	100.0	65.8
27	0	-1	1	0	7.0	0.05	35.0	120.0	104.2
28	1	0	-1	0	9.0	0.07	35.0	80.0	53.2
29	-1	0	1	0	5.0	0.07	35.0	120.0	69.4

established. The wavelength adopted for acidic sample was 278 nm, while 298 nm was used for the basic samples.

## Results and discussion

### Characterization of Co-modified MCM-41

Small-angle X-ray diffraction analyses were used to investigate the structure of as-synthesized materials. As seen from Fig. 1, all the samples exhibit an intense main diffraction peak at  $2\theta$  angle of ca.  $2.3^\circ$  and two weak diffraction peaks at  $2\theta$  angles between  $3^\circ$  and  $5^\circ$ . Compared with MCM-41, the diffraction peaks of Co-MCM-41 became weaker and broader with the increasing of cobalt contents. The XRD patterns can be indexed to hexagonal phase MCM-41 mesoporous

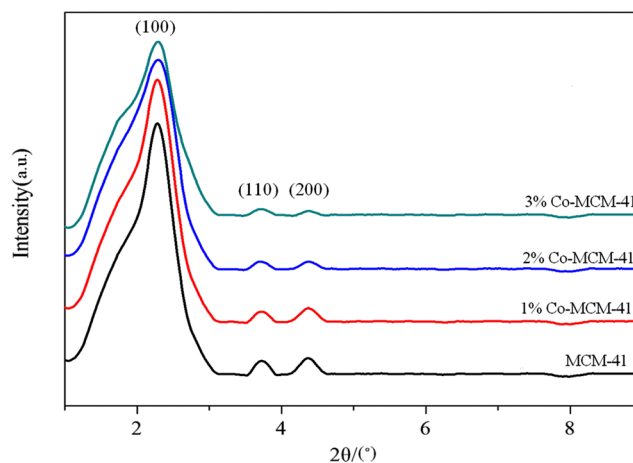


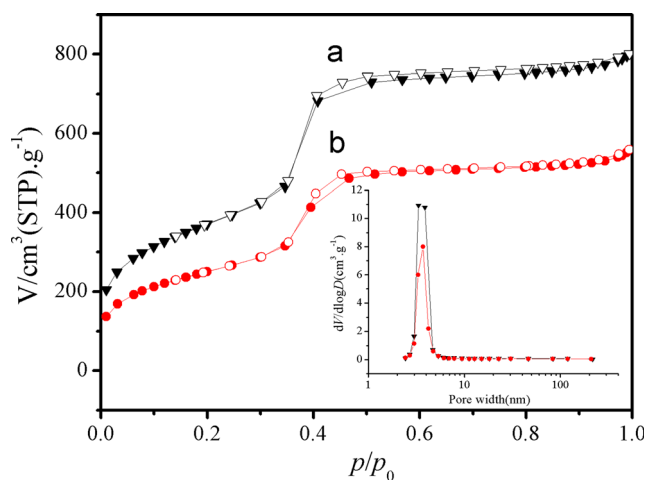
**Fig. 1** Small-angle XRD patterns of MCM-41 and cobalt-modified MCM-41



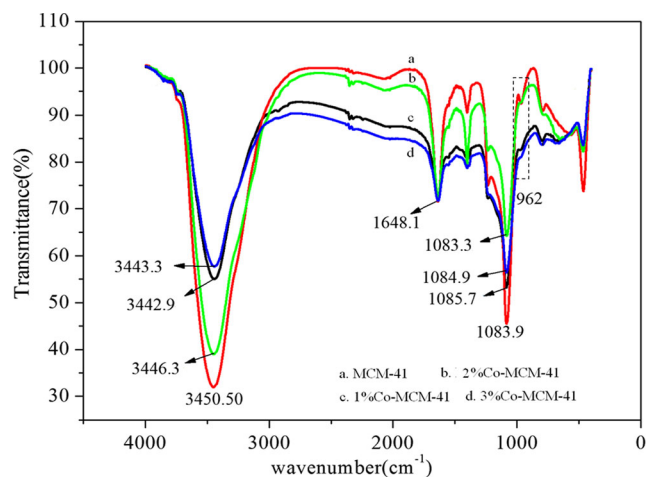
molecular sieve (Ho et al. 2003; Zhao et al. 2009). Thus, it can be deduced that Co-MCM-41 samples still retained the ordered two-dimensional hexagonal mesoporous structure. Nevertheless, the decrease in the peak intensities of Co-MCM-41 materials reveals that the regularity of the structure concurrently decreased due to doping cobalt ions.

Figure 2 shows  $N_2$  adsorption/desorption isotherms of MCM-41 and 3% Co-MCM-41. One can see that both samples display the same adsorption isotherm characteristics: type IV adsorption isotherm with a H2 hysteresis loop. The type IV isotherm suggests that both samples possess mesoporous feature (Dimos et al. 2009; Zhao et al. 2009). The pore size distributions of the samples were inserted in Fig. 2. The narrow pore size distribution curves are evident. The average pore diameters of MCM-41 and 3% Co-MCM-41 are about 3.6 and 3.7 nm, respectively. The increase of pore size indicates that cobalt was incorporated in the silica framework (Lim et al. 2003). The Co–O bond length is longer than that of Si–O. As a result, the longer Co–O bond led to an increasing pore size (Lim et al. 2003). The BET surface areas of MCM-41 and 3% Co-MCM-41 are 1323.13 and 898.55  $m^2 g^{-1}$ , respectively.

Furthermore, the mesoporous structure of 3% Co-MCM-41 was confirmed by FTIR analysis. Gu et al. (1999) proved that infrared absorption peak at around  $961 cm^{-1}$  was related solely with mesoporous structure of the MCM-41 molecular sieve. As expected, this peak was readily detected in MCM-41, 1% Co-MCM-41, 2% Co-MCM-41, and 3% Co-MCM-41 samples (Fig. 3). UV–Vis absorption spectroscopy is very sensitive to chemical state of metal ions and thus was employed to investigate the local environment of cobalt in Co-MCM-41 samples. From Fig. S1 in Supplementary material, one can see that compared with MCM-41, Co-MCM-41



**Fig. 2** Adsorption (solid symbol)/desorption (empty symbol) isotherms of  $N_2$  onto **a** MCM-41 and **b** 3% Co-MCM-41. The inserted figures are the corresponding pore size distribution determined by the BJH method



**Fig. 3** FTIR spectra of MCM-41 and Co-MCM-41 (**a**, MCM-41; **b**, 2% Co-MCM-41; **c**, 1% Co-MCM-41; **d**, 3% Co-MCM-41)

exhibited two discernable absorption bands at 200–250 and 500–650 nm. The former band was ascribed to charge transfer from oxygen to cobalt ions while the later was assigned to tetrahedral coordinated  $Co^{2+}$ . These results also indicate that  $Co^{2+}$  was likely to exist in the silica framework (Lim et al. 2003; Qi et al. 2013). Moreover, the morphological characterization of the synthesized adsorbent was observed from SEM measurements. A representative SEM image of 3% Co-MCM-41 is presented in Fig. 4. It can be seen that 3% Co-MCM-41 consists of large numbers of irregular plates with size about 80 nm. The irregular plates were interconnected and fused together, forming porous agglomerates.

### Adsorption kinetics

Adsorption kinetics is one of the important characteristics that affect adsorption efficiency. Figure 5 shows the uptake of LVF by 3% Co-MCM-41 as a function of contact time. As seen in Fig. 5, a rapid adsorption was observed to take place at the first 30 min, and then followed by a slower adsorption process. The adsorption equilibrium was

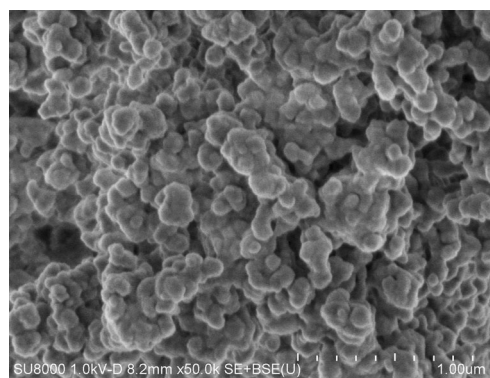


**Fig. 4** FE-SEM image of 3% Co-MCM-41 powder

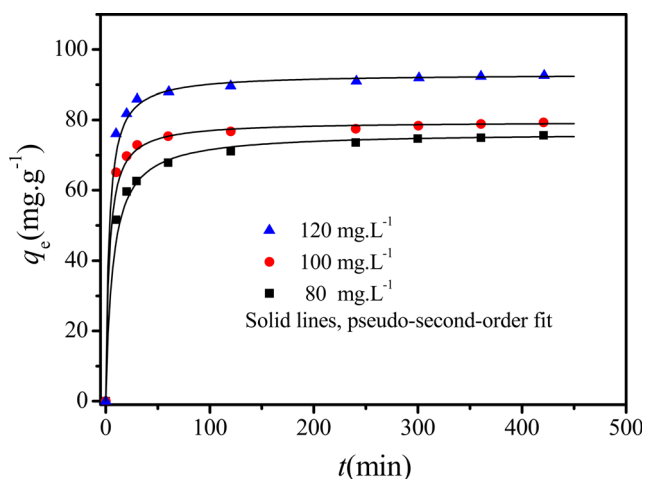


**Fig. 5** Effect of contact time on the adsorption of LVF by 3% Co-MCM-41 (pH = 6.8)

attained within 2 h. The molecule dimensions of LVF are unavailable at the present time. Masson et al. (2016) reported that ofloxacin is 0.52 nm in width and 0.85 nm<sup>3</sup> in volume. Hereby, the larger pore size of 3% Co-MCM-41 may be responsible for its rapid adsorption to LVF. In addition, Carabineiro et al. (2011) demonstrated that carbon-base materials (activated carbons, carbon nanotubes, and carbon xerogels) had high adsorption capacity to CIP. However, a longer period of time (about 3 days) was needed for equilibrium. In this regard, 3% Co-MCM-41 is superior to carbon material for LVF removal due to less mass transfer limitation.

To further estimate adsorption rate and insights into the mechanisms of adsorption reaction, the pseudo-second-order kinetic model was employed to analyze dynamic data. The model is expressed as follows (Ho and McKay 1999):

$$q_t = \frac{q_e^2 k_2 t}{1 + q_e k_2 t} \tag{2}$$

where  $q_e$  and  $q_t$  are the amount of LVF adsorbed (mg g<sup>-1</sup>) at equilibrium and at time  $t$  (min),  $k_2$  is the pseudo-second-order rate constant (g mg<sup>-1</sup> min<sup>-1</sup>).

The plot of pseudo-second-order kinetics for LVX adsorption on 3% Co-MCM-41 is also displayed in Fig. 5 as the solid lines and the fitting results by using the nonlinear method are presented in Table 2 along with the corresponding average relative errors (ARE), which is defined as follows:

$$ARE(\%) = \frac{1}{n} \sum_{i=1}^n \left| \frac{q_{exp} - q_{pre}}{q_{exp}} \right| \times 100 \tag{3}$$

where  $n$  is the number of experimental data points,  $q_{exp}$  is the experimental mass of LVF adsorbed,  $q_{cal}$  is the amount of LVF adsorbed predicted from the model. It is obvious that the pseudo-second-order rate equation fitted the kinetic data fairly

well with the coefficients of determination  $R^2 > 0.99$  and ARE < 2.42%. The adsorption kinetics followed the pseudo-second-order model, indicating a chemisorption process (Shi et al. 2013; Azzaz et al. 2016).

**Optimization and evaluation of the process variables by RSM**

*Building regression model*

A total of 29 experimental runs with five replications at the central point were carried out to study the effect of four independent variables on LVF adsorption by 3% Co-MCM-41. The corresponding adsorption capacities were determined and listed in Table 1 as the observed responses. From these data, a semiempirical second-order polynomial model Eq. (4) was obtained and expressed as follows:

$$y = 65.67 + 4.26x_1 - 17.88x_2 + 12.73x_3 - 1.38x_4 - 1.24x_1x_2 + 2.03x_1x_3 + 1.25x_1x_4 - 3.08x_2x_3 + 0.99x_2x_4 + 0.025x_3x_4 - 3.38x_1^2 + 5.69x_2^2 + 0.41x_3^2 - 1.98x_4^2 \tag{4}$$

where  $y$  is the response variable;  $x_1$ ,  $x_2$ ,  $x_3$ , and  $x_4$  are the independent variables in coded unit, i.e., initial pH, adsorbent dose, LVF concentration, and temperature, respectively.

The significance and adequacy of the response surface quadratic model and model terms were validated by analysis of variance (ANOVA). The results are summarized in Table S1 in the Supplementary material. The large value of Fisher’s  $F$  value of 66.96 of the quadratic model implies that most of the variation in the response can be reasonably explained by the model. The associated  $p$  value (probability >  $F$ ) (< 0.0001) further confirms the statistical significance of the model (Azzaz et al. 2016). The determination coefficient ( $R^2$ ) is often used to verify the fit of the model (Azzaz et al. 2016). The values of  $R^2$  (0.9853), adjusted  $R^2$  (0.9706), and predicted  $R^2$  (0.9166) are close to 1, suggesting a high correlation between the predicted and actual values, which is further signified by plotting the predicted values versus the experimental values in Fig. 6. In addition, an adequate precision of 32.4 also indicates the validity of the model (Amini et al. 2009). All these results reveal that this model can be used to manipulate the design space. From the model, the predicted adsorption capacity (108.1 mg g<sup>-1</sup>) and optimum condition (pH 8.5, adsorbent dosage 1 g L<sup>-1</sup>, LVF concentration 119.8 mg L<sup>-1</sup>, temperature 31.6 °C) were determined. A confirmatory experiment was performed to validate the reliability of the quadratic model. The adsorption capacity of 108 mg g<sup>-1</sup> was obtained at the optimum condition, which is very consistent with the predicted value.

**Table 2** Pseudo-second-order kinetic model parameters for adsorption of LVF on 3% Co-MCM-41

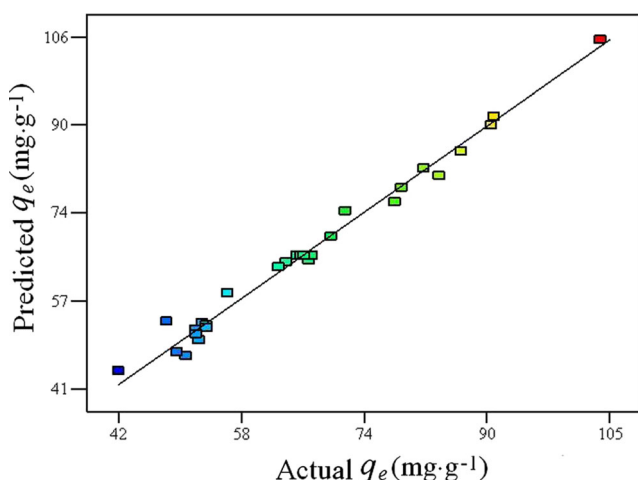
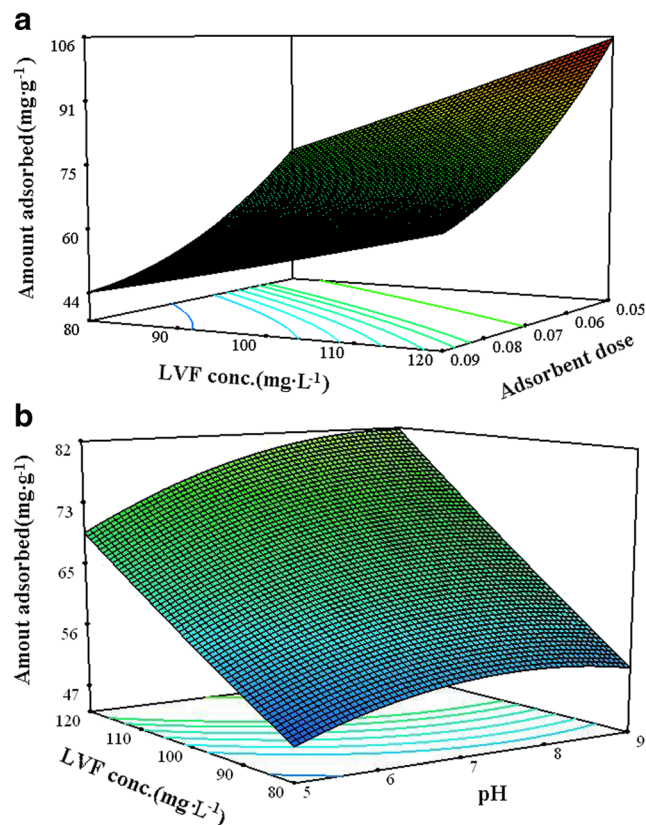
Initial concentration of LVF ( $\text{mg L}^{-1}$ )	$q_e(\text{mg g}^{-1})$	$k_2 (\times 10^{-3} \text{ g mg}^{-1} \text{ min}^{-1})$	ARE (%)	$R^2$
80	76.51	1.98	2.42	0.9998
100	79.62	3.91	1.68	0.9999
120	93.02	3.34	1.62	0.9999

### Interactive effects of process variables

The significance of each coefficient in the model was checked by the  $F$  values and  $p$  value. The large  $F$  value and small probability value indicate that the individual terms in the model have significance on the effect (Azzaz et al. 2016). Generally, the  $p$  value less than 0.05 indicates that the model term is statistically significant at 95% confidence. In this case, the coefficients of  $x_1$ ,  $x_2$ ,  $x_3$ ,  $x_2x_3$ ,  $x_1^2$ , and  $x_2^2$  are statistically significant. Thus, pH, adsorbent dosage, initial concentration of LVF, the interactive effect between adsorbent dosage and the initial concentration of LVF, the square of pH, and the square of the effect of adsorbent dosage have the remarkable effect on LVF adsorption. In contrast, the other factors displayed the insignificant effects on the adsorption process.

The 3D response surface plots are drawn to visualize the combined effect of independent variables on the process response. Except the interactive effects between initial pH and LVF concentration and LVF concentration and adsorbent dose, the other combined effects are not significant even at  $p$  value of 0.15. Therefore, Fig. 7 only presents two pairs of the interactive effects. It can be seen that increasing LVF concentration at a fixed low level adsorbent dose enhances the adsorption capacity intensely while increasing LVF concentration in high level of adsorbent dose slightly affects the

adsorption capacity (Fig. 7a). Moreover, at a low level of LVF concentration, increasing adsorbent concentration leads to a little decrease in the adsorption capacity, whereas it strongly declines at high level of LVF concentration. The decrease in the adsorption capacity with the increase of adsorbent dosage could be ascribed to a “screen” effect on the dense outer layer protecting the binding sites from adsorbate and consequently lowering the specific adsorption capacity at higher adsorbent loading, while the increase in the adsorption capacity with increasing LVF concentration could be explained by strengthening adsorption driving force at high concentration of LVF. The similar results were also reported by other researchers (Kumar et al. 2008; Amini et al. 2009). Figure 7b shows that the adsorption capacity increased with

**Fig. 6** Correlation between the experimental and model-predicted adsorption capacity of LVF**Fig. 7** Response surface plots showing **a** the effect of LVF concentration and adsorbent dosage and their mutual effect and **b** the effect of pH and LVF concentration and their mutual effect on the removal capacity while the other variable at its zero level

raising initial solution pH from 5 to 9 in the entire concentration range of LVF studied. The improved effects were evident in the pH range of 5–7. Above pH 7, the adsorption capacity was improved slightly by increasing solution pH. The concentration of LVF on the adsorption process was same as described above. The effect of solution pH on the observed adsorption behavior of LVF could be explained by taking into account pH-dependent speciation of LVF and surface charge characteristics of the adsorbent. LVF is a zwitterionic compound with acid dissociation constants of 6.2 ( $pK_{a1}$ ) and 8.2 ( $pK_{a2}$ ) (Witte et al. 2009). At  $6.2 \leq \text{pH} \leq 8.2$ , LVF mainly exists in its zwitterionic form in the solution; at  $\text{pH} > 8.2$  or  $< 6.2$ , LVF exists in cationic or anionic form in the solution, respectively. Meanwhile, the point of zero charge (PZC) of Co-doped MCM-41 was about 5.8 (Venezia et al. 2009). Hence, when the solution pH was below 5.8, the surface of adsorbent became positively charged. The repulsion between adsorbent surface and cationic LVF resulted in lowering adsorption of LVF. At  $6.2 < \text{pH} < 8.2$ , LVF is dominated by the zwitterionic form, and adsorption on 3% Co-MCM-41 was favored as previously discussed (Goynes et al. 2005; Gu and Karthikeyan 2005; Li et al. 2011; Shi et al. 2013; Wu et al. 2010), probably due to the other interaction mechanism coupled with the hydrophobic interaction. Several studies have shown that the adsorption of FQs such as ciprofloxacin and ofloxacin onto minerals declined drastically at pH larger than their  $pK_{a2}$ . But this is not the case in this study, indicating that the chemical interaction, rather than electrostatic interaction, was a main mechanism responsible for LVF adsorption on 3% Co-MCM-41.

**Adsorption isotherm and thermodynamics**

Adsorption isotherm can be used to evaluate the adsorption capacity of an adsorbent and get insight into the interaction of an adsorbate and adsorbent. Three typical isotherm models, Langmuir, Freundlich, and Dubinin–Radushkevich (D-R) isothermal equations, are adopted to analyze isotherm data of LVF adsorption on 3% Co-MCM-41, and the models are often written as follows (de Luna et al. 2013):

$$q_e = \frac{q_{\max} K_L C_e}{1 + K_L C_e} \tag{5}$$

$$q_e = K_F C_e^{1/n} \tag{6}$$

$$q_e = q_s \exp(-K_{DR} \varepsilon^2) \tag{7}$$

$$\varepsilon = RT \ln \left( 1 + \frac{1}{C_e} \right) \tag{8}$$

where  $C_e$  is the equilibrium concentration.  $q_e$ ,  $q_{\max}$ , and  $q_s$  are the equilibrium adsorption capacity, maximum adsorption capacity, and the theoretical saturation capacity ( $\text{mg g}^{-1}$ ), respectively.  $K_L$  is the Langmuir adsorption equilibrium constant ( $\text{L mg}^{-1}$ ), which is related to the binding energy of the adsorption system;  $K_F$  ( $\text{mg}^{1-n} \text{L}^n \text{g}^{-1}$ ) and  $1/n$  are the Freundlich

constants, which are indicative of the adsorption capacity and the surface site heterogeneity of the adsorbent, respectively.  $K_{DR}$  is the constant ( $\text{mol}^2 \text{kJ}^{-2}$ ), and  $\varepsilon$  is the Polanyi potential. The mean free energy of adsorption ( $E$ ) is calculated from  $E = (2K_{DR})^{-1/2}$ .

Figure 8 and Table 3 display fitting of isotherm data to Langmuir, Freundlich, and D-R models using nonlinear regression method. It is seen that all of these isothermal models could effectively describe the adsorption data due to their larger coefficient of determination ( $R^2 > 0.98$ ). Nevertheless, D-R model in all cases provided the best fit due to the larger coefficients of determination and lower average relative errors. The maximum adsorption capacity (i.e.,  $q_{\max}$  obtained from the Langmuir model) of 3% Co-MCM-41 for LVF at room temperature was about  $0.29 \text{ mmol g}^{-1}$ . Compared with the adsorption capacity of goethite ( $0.06 \text{ mmol g}^{-1}$  for CIP) (Gu and Karthikeyan 2005), aluminum hydrous oxide ( $0.041 \text{ mmol g}^{-1}$  for CIP) (Gu and Karthikeyan 2005), kaolinite ( $0.019 \text{ mmol g}^{-1}$  for CIP) (Li et al. 2011), montmorillonite ( $1.2 \text{ mmol g}^{-1}$  for CIP) (Wu et al. 2010), magnetic mesoporous carbon composite ( $0.29 \text{ mmol g}^{-1}$  for CIP) (Shi et al. 2013), carbon materials ( $0.18\text{--}0.91 \text{ mmol g}^{-1}$  for CIP) (Carabineiro et al. 2011), modified coal fly ash ( $0.0078 \text{ mmol g}^{-1}$  for norfloxacin) (Zhang et al. 2010), Si-P700 ( $1.05 \text{ mmol g}^{-1}$  for ofloxacin), Al-P242 ( $0.29 \text{ mmol g}^{-1}$  for ofloxacin) (Goynes et al. 2005), and microporous-activated carbon fabric ( $0.7 \text{ mmol g}^{-1}$  for ofloxacin) (Masson et al. 2016), 3% Co-MCM-41 exhibited a higher adsorption capacity toward LVF. Thus, it is a promising candidate for the removal of LVF in water cleanup.

It is generally believed that Freundlich constant  $1/n > 2$ , showing that the adsorption is more difficult;  $1/n = 1$ , showing a linear adsorption;  $0.1 < 1/n < 0.5$ , showing the process of adsorption is easy. The adsorption constant  $1/n$  in this study was between 0.4 and 0.6, indicating that adsorption of LVF over 3% Co-MCM-41 was prone. D-R model is mainly used

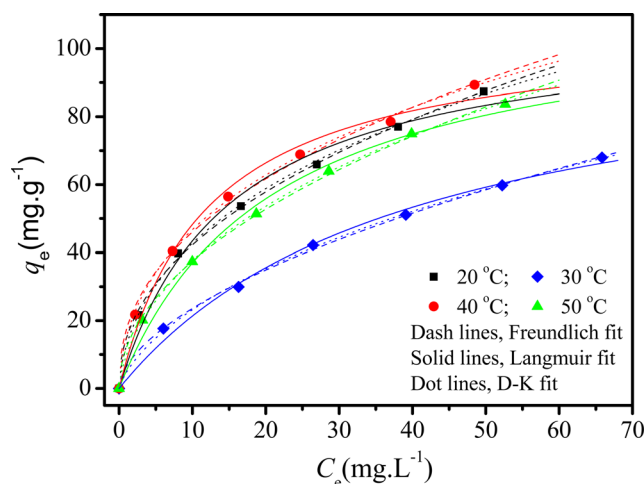


**Fig. 8** Adsorption isotherms of LVF on 3% Co-MCM-41 fitting to Langmuir, Freundlich, and Dubinin–Radushkevich equations



**Table 3** Isotherm parameters for the adsorption of LVF onto 3%Co-MCM-41

T/K	Langmuir				Freundlich				Dubinin–Radushkevich				
	$q_{\max}$ ( $\text{mg g}^{-1}$ )	$K_L$ ( $\text{L mg}^{-1}$ )	$R^2$	ARE (%)	$K_F$ ( $\text{mg}^{1-1/n}$ $\text{L}^{1/n} \text{g}^{-1}$ )	$1/n$	$R^2$	ARE (%)	$q_s$ ( $\text{mg g}^{-1}$ )	$K_{\text{DR}}(\times 10^{-3})$ ( $\text{mol}^2 \text{kJ}^{-2}$ )	$R^2$	ARE (%)	$E$ ( $\text{kJ mol}^{-1}$ )
293.15	108.23	0.067	0.9873	4.67	14.89	0.45	0.9983	2.15	520.19	3.82	0.9986	1.44	11.44
313.15	106.37	0.083	0.9898	6.78	17.37	0.42	0.9954	3.26	473.48	3.33	0.9983	1.62	12.29
333.15	113.96	0.048	0.9927	6.19	12.03	0.49	0.9982	1.82	596.38	3.70	0.9996	0.75	11.62
353.15	106.45	0.025	0.9943	5.17	6.45	0.56	0.9981	1.46	614.11	4.12	0.9982	2.06	11.02

to describe the adsorption behavior of the non-uniform surface. The type of adsorption can be determined from  $E$  value; if  $E$  falls in the range of 8–16  $\text{kJ mol}^{-1}$ , the adsorption is dominated by chemical ion-exchange; if  $E$  is lower than 8  $\text{kJ mol}^{-1}$ , the adsorption is dominated by physical forces (Li et al. 2016).  $E$  values of LVF adsorption over 3% Co-MCM-41 varied from 11.02 to 12.29  $\text{kJ mol}^{-1}$ , which is larger than 8  $\text{kJ mol}^{-1}$ , suggesting that the adsorption is a chemisorption process (Li et al. 2016).

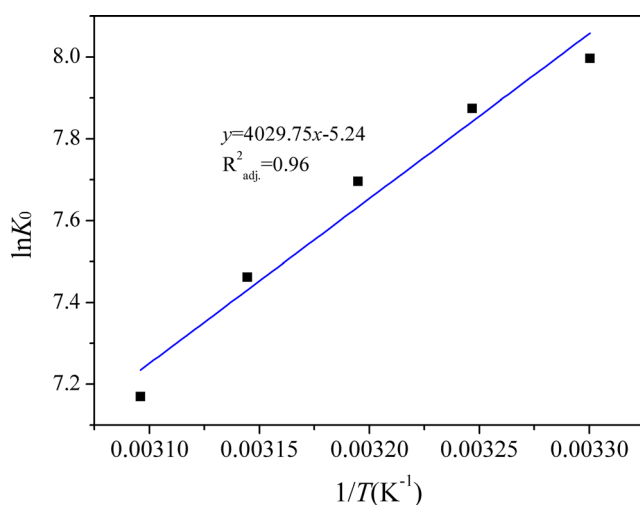
The thermodynamic parameters, such as changes in standard enthalpy ( $\Delta H^0$ ), entropy ( $\Delta S^0$ ), and Gibbs free energy ( $\Delta G^0$ ), are useful for evaluating adsorption process. They can be obtained from the temperature-dependent isothermal data by using the Van't Hoff equation:

$$\ln K_0 = \frac{\Delta S^0}{R} - \frac{\Delta H^0}{RT} \quad (9)$$

and

$$\Delta G^0 = -RT \ln K_0 \quad (10)$$

where  $K_0$  is the adsorption equilibrium constant, determined by plotting  $\ln(q_e/C_e)$  versus  $q_e$  and extrapolating  $q_e$  to 0 (Alam et al. 2005).

**Fig. 9** Van't Hoff plot for estimation of thermodynamic parameters

The plot of  $\ln K_0$  versus  $1/T$  is depicted in Fig. 9;  $\Delta H^0$  and  $\Delta S^0$  were calculated from the slope and intercept of the straight line and tabulated in Table 4. The changes in adsorption enthalpy, entropy, and Gibbs free energy were  $-33.5 \text{ kJ mol}^{-1}$ ,  $-43.57 \text{ J mol}^{-1} \text{ K}^{-1}$ , and  $-19.26$  to  $-20.20 \text{ J mol}^{-1}$ , respectively. The negative  $\Delta H^0$  suggests the exothermic nature of the adsorption interaction, while the negative  $\Delta S^0$  reflects the decreasing randomness at the solid/solution interface during the adsorption process.

## Conclusion

In summary, we have successfully prepared cobalt-modified MCM-41 via a one-pot hydrothermal method. The prepared material was characterized and employed as a novel adsorbent for removal of LVF from aqueous solution. The adsorption process was found to follow pseudo-second-order kinetics. The isotherms could be well described by the Langmuir, Freundlich, and Dubinin–Radushkevich (D-R) isotherm equations. The average adsorption energy ( $E$ ) calculated from D-R model implied that the adsorption was chemisorption. RSM was used to evaluate the effects of the process variables (pH, adsorbent dosage, LVF concentration, temperature) on LVF adsorption and to optimize adsorption condition. A response surface quadratic model was established with  $R^2 = 0.985$ . Under optimal conditions (pH 8.5, adsorbent dosage of  $1 \text{ g L}^{-1}$ , LVF concentration of  $119.8 \text{ mg L}^{-1}$ , temperature of  $31.6 \text{ }^\circ\text{C}$ ), the adsorption capacity of 3% Co-MCM-41 to LVF

**Table 4** Thermodynamic functions for adsorption of LVF on 3% Co-MCM-41

T/K	$K_0$	$\Delta G^0$ ( $\text{kJ mol}^{-1}$ )	$\Delta S^0$ ( $\text{J mol}^{-1} \text{ K}^{-1}$ )	$\Delta H^0$ ( $\text{kJ mol}^{-1}$ )
303	2970	-20.14	-43.57	-33.50
308	2630	-20.16		
313	2200	-20.03		
318	1740	-19.73		
323	1300	-19.26		

could reach  $108.1 \text{ mg g}^{-1}$ . pH, adsorbent dosage, LVF concentration, the mutual interaction between adsorbent loading vs LVF concentration, the square of pH, and the square of adsorbent dosage were found to be significant factors affecting the adsorption behavior of 3% Co-MCM-41 to LVF. The thermodynamic functions of the adsorption process, on the other hand, revealed that the adsorption process was exothermic with decrease of disorder of system. On base of these results, it is expected that 3% Co-MCM-41 is a promising adsorbent for removing emerging pollutants of LVF from water.

**Acknowledgements** The authors gratefully acknowledge the financial supports from NFFTBS (No. J1103311 and No. J1210057) and Open Funding Project of State Key Laboratory Base of Eco-Hydraulic Engineering in Arid Area, Xi'an University of Technology (No. 2016KFKT-3).

## References

- Alam JB, Dikshit AK, Bandyopadhyay M (2005) Evaluation of thermodynamic properties of sorption of 2,4-D and atrazine by tire rubber granules. *Sep Purif Technol* 42:85–90
- Ali I (2010) The quest for active carbon adsorbent substitutes: inexpensive adsorbents for toxic metal ions removal from wastewater. *Sep Purif Rev* 39:95–171
- Ali I (2012) New generation adsorbents for water treatment. *Chem Rev* 112:5073–5091
- Ali I (2014) Water treatment by adsorption columns: evaluation at ground level. *Sep Purif Rev* 43:175–205
- Ali I, Aboul-Enein HY (2004) Chiral pollutants: distribution, toxicity and analysis by chromatography and capillary electrophoresis. John Wiley & Sons, Chichester
- Ali I, Asin M, Khan TA (2012) Low cost adsorbents for the removal of organic pollutants from wastewater. *J Environ Manag* 113:170–183
- Amimi M, Younesi H, Bahramifar N (2009) Biosorption of nickel(II) from aqueous solution by *Aspergillus niger*: response surface methodology and isotherm study. *Chemosphere* 75:1483–1491
- Azzaz AA, Jellali S, Akrouf H, Assadi AA, Boussemli L (2016) Optimization of a cationic dye removal by a chemically modified agriculture by-product using response surface methodology: biomass characterization and adsorption properties. *Environ Sci Pollut Res*. doi:10.1007/s11356-016-7698-6
- Benhamou A, Baudu M, Derriche Z, Basly JP (2009) Aqueous heavy metals removal on amine-functionalized Si-MCM-41 and Si-MCM-48. *J Hazard Mater* 171:1001–1008
- Brain RA, Johnson DJ, Richards SM, Sanderson H, Sibley PK, Solomon KR (2004) Effects of 25 pharmaceutical compounds to *Lemma gibba* using a seven-day static-renewal test. *Environ Toxicol Chem* 23:371–382
- Carabineiro SAC, Thavorn-Amornsri T, Pereira MFR, Figueiredo JL (2011) Adsorption of ciprofloxacin on surface-modified carbon materials. *Water Res* 45:4583–4591
- Chatterjee M, Ishizaka T, Kawanami H (2014) Preparation and characterization of PdO nanoparticles on trivalent metal (B, Al and Ga) substituted MCM-41: excellent catalytic activity in supercritical carbon dioxide. *J Colloid Interf Sci* 420:15–26
- Chen W, Li X, Pan Z, Bao Y, Ma S, Li L (2015) Efficient adsorption of norfloxacin by Fe-MCM-41 molecular sieves: kinetic, isotherm and thermodynamic studies. *Chem Eng J* 281:397–403
- de Luna MDG, Flores ED, Genuino DAD, Futralan CM, Wan M-W (2013) Adsorption of eriochrome black T (EBT) dye using activated carbon prepared from waste rice hulls—optimization, isotherm and kinetic studies. *J Taiwan Inst Chem Eng* 44:646–653
- Dimos K, Stathi P, Karakassides MA, Deligiannakis Y (2009) Synthesis and characterization of hybrid MCM-41 materials for heavy metal adsorption. *Micropor Mesopor Mater* 126:65–71
- Djordjevic P, Milenajelkic-Stankov, Lazarevic L (2001) The effect of surfactants on equilibria in aluminium (III) ion + ofloxacin solution and adsorption of ofloxacin on aluminium - oxide. *Bull Chem Soc Jpn* 74:1261
- Dodd MC, Shah AD, Gunten UV, Huang C (2005) Interactions of fluoroquinolone antibacterial agents with aqueous chlorine: reaction kinetics, mechanisms, and transformation pathways. *Environ Sci Technol* 39:7065–7076
- Goyne KW, Chorover J, Kubicki JD, Zimmerman AR, Brantley SL (2005) Sorption of the antibiotic ofloxacin to mesoporous and non-porous alumina and silica. *J Colloid Interf Sci* 283:160–170
- Gu C, Karthikeyan KG (2005) Sorption of the antimicrobial ciprofloxacin to aluminum and iron hydrous oxides. *Environ Sci Technol* 39:9166–9173
- Gu G, Ong PP, Chu C (1999) Thermal stability of mesoporous silica molecular sieve. *J Phys Chem Solids* 60:943–947
- Halling-Sorensen B, Nielsen NS, Lanzky PF, Ingerslev F, Litzthof HCH, Jorgensen SE (1998) Occurrence, fate and effects of pharmaceutical substances in the environment - a review. *Chemosphere* 36:357–393
- Hartmann A, Alder AC, Koller T, Widmer RM (1998) Identification of fluoroquinolone antibiotics as the main source of umuc genotoxicity in native hospital wastewater. *Environ Toxicol Chem* 17:377–382
- Ho YS, McKay G (1999) Pseudo-second order model for sorption processes. *Process Biochem* 34:451–465
- Ho KY, McKay G, Yeung KL (2003) Selective adsorbents from ordered mesoporous silica. *Langmuir* 19:3019–3024
- Jung C, Son A, Her N, Zoh K-D, Cho J, Yoon Y (2015) Removal of endocrine disrupting compounds, pharmaceuticals, and personal care products in water using carbon nanotubes: a review. *J Ind Eng Chem* 27:1–11
- Kim J-W, Jang H-S, Kim J-G, Ishibashi H, Hirano M, Nasu K, Ichikawa N, Takao Y, Shinohara R, Arizono K (2009) Occurrence of pharmaceutical and personal care products (PPCPs) in surface water from Mankyung river, South Korea. *J Health Sci* 55:249–258
- Kumar R, Bishnoi NR, Garima, Bishnoi K (2008) Biosorption of chromium(VI) from aqueous solution and electroplating wastewater using fungal biomass. *Chem Eng J* 135:202–208
- Li Z, Hong H, Liao L, Ackley CJ, Schulz LA, MacDonald RA, Mihelich AL, Emard SM (2011) A mechanistic study of ciprofloxacin removal by kaolinite. *Colloids Surf B* 88:339–344
- Li A, Pi S, Wei W, Chen T, Yang J, Ma F (2016) Adsorption behavior of tetracycline by extracellular polymeric substrates extracted from *Klebsiella* sp. *J Environ Sci Pollut Res*. doi:10.1007/s11356-016-7726-6
- Lim S, Ciuparu D, Pak C, Dobek F, Chen Y, Harding D, Pfefferle L, Haller G (2003) Synthesis and characterization of highly ordered Co-MCM-41 for production of aligned single walled carbon nanotubes (SWNT). *J Phys Chem B* 107:11048–11056
- Liu Y, Dong C, Wei H, Yuan W, Li K (2015) Adsorption of levofloxacin onto an iron-pillared montmorillonite (clay mineral): kinetics, equilibrium and mechanism. *Appl Clay Sci* 118:301–307
- Martins AR, Salviano AB, Oliveira AA, Mambri RV, Moura FC (2016) Synthesis and characterization of catalysts based on mesoporous silica partially hydrophobized for technological applications. *Environ Sci Pollut Res*. doi:10.1007/s11356-016-6692-3
- Masson S, Vaultot C, Reinert L, Guittonneau S, Gadiou R, Duclaux L (2016) Thermodynamic study of seven micropollutants adsorption onto an activated carbon cloth: Van't Hoff method, calorimetry, and

- COSMO-RS simulations. *Environ Sci Pollut Res*. doi:10.1007/s11356-016-7614-0
- Nowara A, Burhenne J, Spittler M (1997) Binding of fluoroquinolone carboxylic acid derivatives to clay minerals. *J Agric Food Chem* 45: 1459–1463
- Paul T, Miller PL, Strathmann TJ (2007) Visible-light-mediated TiO<sub>2</sub> photocatalysis of fluoroquinolone antibacterial agents. *Environ Sci Technol* 41:4720–4727
- Paul T, Dodd MC, Strathmann TJ (2010) Photolytic and photocatalytic decomposition of aqueous ciprofloxacin: transformation products and residual antibacterial activity. *Water Res* 44:3121–3132
- Peng H, Pan B, Wu M, Liu R, Zhang D, Wu D, Xing B (2012) Adsorption of ofloxacin on carbon nanotubes: solubility, pH and cosolvent effects. *J Hazard Mater* 211–212:342–348
- Perini JAL, Silva BC, Tonetti AL, Nogueira RFP (2016) Photo-Fenton degradation of the pharmaceuticals ciprofloxacin and fluoxetine after anaerobic pre-treatment of hospital effluent. *Environ Sci Pollut Res*. doi:10.1007/s11356-016-7416-4
- Punyapalaku P, Sitthisorn T (2010) Removal of ciprofloxacin and carbamazepine by adsorption on functionalized mesoporous silicates. *World Acad Sci Eng Technol* 69:546–550
- Qi F, Chu W, Xu B (2013) Catalytic degradation of caffeine in aqueous solutions by cobalt-MCM41 activation of peroxymonosulfate. *Appl Catal B* 134–135:324–332
- Robinson AA, Belden JB, Lydy MJ (2005) Toxicity of fluoroquinolone antibiotics to aquatic organisms. *Environ Toxicol Chem* 24:423–430
- Roosta M, Ghaedi M, Asfaram A (2015) Simultaneous ultrasonic-assisted removal of malachite green and safranin O by copper nanowires loaded on activated carbon: central composite design optimization. *RSC Adv* 5:57021–57029
- Serna-Galvis EA, Giraldo-Aguirre AL, Silva-Agredo J, Florez-Acosta OA, Torres-Palma RA (2016) Removal of antibiotic cloxacillin by means of electrochemical oxidation, TiO<sub>2</sub> photocatalysis, and photo-Fenton processes: analysis of degradation pathways and effect of the water matrix on the elimination of antimicrobial activity. *Environ Sci Pollut Res*. doi:10.1007/s11356-016-6257-5
- Sharma VK (2008) Oxidative transformations of environmental pharmaceuticals by Cl<sub>2</sub>, ClO<sub>2</sub>, O<sub>3</sub>, and Fe(VI): kinetics assessment. *Chemosphere* 73:1379–1386
- Shi S, Fan Y, Huang Y (2013) Facile low temperature hydrothermal synthesis of magnetic mesoporous carbon nanocomposite for adsorption removal of ciprofloxacin antibiotics. *Ind Eng Chem Res* 52:2604–2612
- Van Doorslaer X, Dewulf J, Van Langenhove H, Demeestere K (2014) Fluoroquinolone antibiotics: an emerging class of environmental micropollutants. *Sci Total Environ* 500–501:250–269
- Venezia AM, Murania R, Pantaleo G, La Parola V, Scirè S, Deganello G (2009) Combined effect of noble metals (Pd, Au) and support properties on HDS activity of Co/SiO<sub>2</sub> catalysts. *Appl Catal A* 353:296–304
- Wei H, Hu D, Su J, Li K (2015) Intensification of levofloxacin sonodegradation in a US/H<sub>2</sub>O<sub>2</sub> system with Fe<sub>3</sub>O<sub>4</sub> magnetic nanoparticles. *Chinese J Chem Eng* 23:296–302
- Witte BD, Langenhove HV, Hemelsoet K, Demeestere K, Wispelaere PD, Van Speybroeck V, Dewulf J (2009) Levofloxacin ozonation in water: rate determining process parameters and reaction pathway elucidation. *Chemosphere* 76:683–689
- Wu Q, Li Z, Hong H, Yin K, Tie L (2010) Adsorption and intercalation of ciprofloxacin on montmorillonite. *Appl Clay Sci* 50:204–211
- Xiao X, Zeng X, Lemley AT (2010) Species-dependent degradation of ciprofloxacin in a membrane anodic Fenton system. *J Agric Food Chem* 58:10169–10175
- Xu X, Wu J, Xu W, He M, Fu M, Chen L, Zhu A, Ye D (2016) High-efficiency non-thermal plasma-catalysis of cobalt incorporated mesoporous MCM-41 for toluene removal. *Catal Today*. doi:10.1016/j.cattod.2016.03.036
- Zhang C, Li B, Wang Y (2010) Adsorption of norfloxacin from aqueous solution onto modified coal fly ash. *Chem Eng Technol* 33:969–972
- Zhao Q, Xu Y, Li Y, Jiang T, Li C, Yin H (2009) Effect of the Si/Ce molar ratio on the textural properties of rare earth element cerium incorporated mesoporous molecular sieves obtained room temperature. *Appl Surf Sci* 255:9425–9429